arXiv:1106.1586v1 [physics.chem-ph] 8 Jun 2011

Rotational spectrum of asymmetric top molecules in combined static and laser fields

J. J. Omiste,[1] R. González-Férez,[1] and P. Schmelcher[2]

[1]*Instituto Carlos I de Física Teórica y Computacional, and Departamento de Física Atómica, Molecular y Nuclear, Universidad de Granada, 18071 Granada, Spain*

[2]*Zentrum für Optische Quantentechnologien, Luruper Chaussee 149, Universität Hamburg, 22761 Hamburg, Germany*

(Dated: January 28, 2013)

We examine the impact of the combination of a static electric field and a non resonant linearly polarized laser field on an asymmetric top molecule. Within the rigid rotor approximation, we analyze the symmetries of the Hamiltonian for all possible field configurations. For each irreducible representation, the Schrödinger equation is solved by a basis set expansion in terms of a linear combination of Wigner functions respecting the corresponding symmetries, which allows us to distinguish avoided crossings from genuine ones. Using the fluorobenzene and pyridazine molecules as prototypes, the rotational spectra and properties are analyzed for experimentally accessible static field strengths and laser intensities. Results for energy shifts, orientation, alignment and hybridization of the angular motion are presented as the field parameters are varied. We demonstrate that a proper selection of the fields gives rise to a constrained rotational motion in the three Euler angles, the wave function being oriented along the electrostatic field direction, and aligned in the other two angles.

I. INTRODUCTION

The manipulation of large molecules by using external fields represents, in spite of its long history, a very active and promising research area. Indeed, major efforts have been undertaken to create samples of oriented and/or aligned molecules, and a large variety of experimental techniques have been developed, such as, e.g., the brute force orientation [1], hexapole focusing [2–4], a train of laser pulses [5, 6], or a combination of a laser pulse and a weak static electric field [7–9]. The control and manipulation of the directional features of molecules, i.e., of their rotational degree of freedom, optimize the information content on experimental measurements performed in the laboratory frame. Indeed, the availability of asymmetric top molecules in oriented and/or aligned pendular states allows for a wealth of interesting applications in areas as diverse as spectroscopy [10, 11], photoelectron angular distributions [12, 13], sterodynamic control of chemical reactions [14–17], dissociation of molecules [18–21], electron diffraction [22], or high-harmonic generation [23, 24].

The experimental achievements have been accompanied by theoretical efforts to understand and explain the intriguing physical phenomena appearing in asymmetric top molecules exposed to external fields. Regarding the impact of radiative fields on these molecules, the corresponding theoretical studies have been especially fruitful in explaining a vast amount of experimental results, such as, e.g., the rotational revival structure following the irradiation by an intense picosecond laser pulses [25], the three-dimensional alignment by elliptically polarized laser fields [26–28] or the use of long and short laser pulses to control the rotation [29, 30]. Analogously, the motivation of the theoretical works considering an electrostatic field was either to interpret some experimental results [10], or to confirm the feasibility of other experiments, e.g., the Stark deceleration of polyatomic asymmetric molecules [31]. The molecular orientation due to the interaction with a static electric field has been investigated for asymmetric top molecules with their permanent dipole moment $\boldsymbol{\mu}$ parallel to a principal axis of inertia, and for the non-parallel case [4, 32, 33]. In the strong electrostatic field regime, an analytical study of the energy-level representation has shown that the asymmetric top pendular states are well described by a two-dimensional anisotropic harmonic oscillator [34], and it has been used to reproduce spectroscopic results in the pendular regime for static fields up to 200 kVcm^{-1} [11].

A detailed analysis of the rotational spectrum of symmetric top molecules exposed to combined electrostatic and nonresonant radiative fields was recently performed by Härtelt and Friedrich [35]. For tilted fields, only the projection of the total angular momentum $\mathbf{J}$ onto the body fixed frame z-axis K remains as good quantum number, and a 2D description of the rotational spectrum of the molecule is required. The corresponding dynamics is very complicated, indeed, in the presence of a static electric field, it has been shown that the molecular spectrum presents classical and quantum monodromy [36]. They provide correlation diagrams between the field-free states and the pendular levels of the intense laser field [37] as well as the strong electrostatic field regime. For a selection of states, they investigate the energy shifts and directional properties (orientation and alignment) for parallel and perpendicular fields. In these systems, the coupling of both field interactions could provoke an enhancement of the orientation giving rise to an oriented and antioriented pair of levels. For an oblate system, this phenomenon appears in the tunneling doublets created by the interaction of the molecular polarizability with the linear polarized laser field (this effect was already analyzed for linear molecules [38–40]), whereas for a prolate molecule, it appears among exactly degenerate doublets of indefinite parity appearing in the strong laser field regime.

A classical theoretical analysis of asymmetric top molecules exposed to a combination of static and laser fields has been performed recently [41]. However, the quantum analog has not yet been addressed in the literature, to the best of our knowledge. Recently, the authors have developed a diabatic model to describe the evolution of alignment and orientation of asymmetric top molecules in combined fields as the laser intensity is varied [42]. The outcome of this theoretical study has been compared to the experimental data obtained for the benzonitrile molecule [13] proving the importance of non-adiabatic processes in the field-dressed molecular dynamics. Thus, motivated by the current experimental interest on these asymmetric molecules [7–9, 12, 13] and by the fact that the rotational dynamics of most polyatomic molecules can be described as asymmetric tops, we extend in the present work the previous study on symmetric tops [35] to these more complicated systems. We perform a theoretical investigation of an asymmetric top in the presence of combined electrostatic and nonresonant radiative fields within the rigid rotor description. The field-dressed rotational spectrum is significantly more complicated, and the more general case of no collinear field requires a full 3D description. We will perform a detailed analysis of the symmetries of the Hamiltonian for all possible field configurations. In tilted fields, the reduction of the symmetries enhances the complexity of the spectrum, and a large amount of avoided crossing appears between states of the same symmetry. Hence, to simplify the analysis and interpretation of our results, the Schrödinger equation is numerically solved for each irreducible representation by expanding the wave function in a basis with the corresponding symmetry. As prototype examples we consider (C_6H_5F) and pyridazine ($C_4H_4N_2$) molecules. These two systems have similar values of their polarizability tensors and dipole moments, but different inertia tensors and are, therefore, affected differently by the external fields. We explore their rotational spectrum as either the laser intensity, the electrostatic field strength, or the inclination angle between them is varied. Our focus is on the energy shifts, the directional properties and the hybridization of the angular motion. Depending on the dominant interaction, a rich field-dressed dynamics is observed with levels achieving different degrees of orientation and/or alignment. The role played by the inclination angle is exemplary investigated via a set of states and in avoided crossings between two adjacent levels. Moreover, we show that due to the combination of both field interactions the rotational motion is restricted in the three Euler angles, being oriented along the static electric field direction and constrained in the XY plane of the laboratory frame, which is perpendicular to the laser polarization. This mechanism of orientation and 2D alignment is very sensitive to the field parameters and to the molecular properties.

The paper is organized as follows. In Sec. II the rotational Hamiltonian is presented together with a comprehensive consideration of its symmetries for the different field configurations. In Sec. III, we discuss the numerical results for two asymmetric molecules, fluorobenzene and pyridazine, as the field parameters are modified. In particular, we explore three different cases: i) for fixed laser intensity and three inclination angles, we vary the electrostatic field strength; ii) for fixed electrostatic field and three inclination angles the laser intensity is enhanced; and iii) for fixed laser intensity and electrostatic field strengths, the angle between them is continuously changed from 0 to $\pi/2$. The conclusions and outlook are provided in Sec. IV.

II. HAMILTONIAN OF AN ASYMMETRIC TOP MOLECULE IN THE PRESENCE OF THE FIELDS

We consider a polar and polarizable asymmetric top molecule exposed to an homogeneous static electric field and a nonresonant linearly polarized laser. Our study is restricted to the regime of field strengths that significantly affects the rotational dynamics of the molecule, whereas its impact on the electronic and vibrational structure can be described by first order perturbation theory. We work within the Born-Oppenheimer approximation, assuming that the rotational and vibrational dynamics can be adiabatically separated, and apply a rigid rotor description of the molecular systems. Furthermore, we neglect relativistic, fine and hyperfine interactions as well as couplings of different electronic states. In the laboratory fixed frame (LFF) (X, Y, Z), the Z-axis is chosen parallel to the polarization of the laser, and the direction of the homogenous electric field is taken forming an angle β with this axis and contained in the XZ plane. The molecular or body fixed frame (MFF) (x, y, z) is defined so that the permanent electric dipole moment is parallel to the z-axis, and for the considered systems the smallest moment of inertia is parallel to the x-axis. The relation between both frames is given by the Euler angles $\Omega = (\phi,\ \theta,\ \chi)$ [43], which are shown together with the field configurations in Fig. 1. We only analyze molecules having the electric dipole moment parallel to one of the axis, and a diagonal polarizability tensor. Thus, the rigid rotor Hamiltonian reads

$$H = H_r + H_S + H_L, \tag{1}$$

where H_r is the field-free Hamiltonian, and H_S and H_L stand for the interactions with the static and the laser field, respectively.

In the absence of the fields, the rigid rotor Hamiltonian is given by

$$H_r = B_x J_x^2 + B_y J_y^2 + B_z J_z^2 \tag{2}$$

where the angular momentum operators refer to the MFF, with $B_i = \hbar^2/2I_{ii}$ being the rotational constant and I_{ii} the moment of inertia around the principal axis of inertia i, with $i = x, y$ and z. An estimation of the degree of asymmetry is provided by Ray's parameter, $\kappa = (2B_y - B_z - B_x)/(B_y - B_x)$, where the rotational constants of the considered system satisfy $B_z \geq B_y \geq B_x$. For a symmetric top ($B_x = B_y$), Ray's parameter takes the extreme values $\kappa = 1$ and -1 for the oblate and prolate cases, respectively.

For the regime of electrostatic field strengths $\mathbf{E_S}$ considered here, we can neglect the interaction via the molecular polarizability, arriving at the following the Stark Hamiltonian

$$H_S = -\mathbf{E_S} \cdot \boldsymbol{\mu} = -E_S \mu \cos\theta_S, \tag{3}$$

where θ_S is the angle between the permanent molecular electric dipole moment, $\boldsymbol{\mu} = \mu\hat{\mathbf{z}}$, and the static electric field with $\cos\theta_S = \cos\beta\cos\theta + \sin\beta\sin\theta\cos\phi$ and $0 \leq \beta \leq \pi/2$.

Here, we consider a nonresonant laser field linearly polarized along the Z axis, $\mathbf{E_L}(t) = E_{\text{max}} g(t)\cos(2\pi\nu t)\mathbf{Z}$, with the frequency ν, the field strength E_{max}, and $g(t)$ being the pulse envelope. We assume that ν^{-1} is much shorter than the pulse duration or the rotational period, so that we can average over the rapid oscillations, which causes the coupling of this field with the permanent dipole moment to vanish [44, 45]. In addition, we assume that the pulse duration is much longer than the rotational period of the molecular system, such that the states adiabatically follow the change of the field, and we restrict our analysis to the adiabatic limit $g(t) \to 1$. Hence, the interaction of the laser with the polarizability is the leading order term, and can be written as

$$H_L = -\frac{I}{2c\epsilon_0}(\alpha^{zx}\cos^2\theta + \alpha^{yx}\sin^2\theta\sin^2\chi) \tag{4}$$

with $\alpha^{ji} = \alpha_{jj} - \alpha_{ii}$, and α_{ii} being the i-th diagonal element of the polarizability tensor, with $i = x,\ y,\ z$ [46]. In this expression we have used $\langle E_L^2\rangle = I/c\epsilon_0$, c being the speed of light, ϵ_0 the dielectric constant, and expectation value $\langle E_L^2\rangle$ indicates the time average.

Our aim is to investigate the rotational spectrum of an asymmetric top molecule exposed to different field configurations. To do so, we solve the time-independent Schrödinger equation associated to the Hamiltonian (1), which even in the field-free case can not be solved analytically. Let us start by analyzing how the symmetries of this Hamiltonian change when the angle between the fields varies.

A. Symmetries

A detailed analysis of the symmetries of an asymmetric top rotor in the field-free case and exposed to a static electric field has been performed in Ref. 34. Here, we extend this study to the field configurations investigated in this work.

The symmetries of the field-free Hamiltonian (2) are the spatial SO(3) rotation group and a subgroup of this group relevant to the symmetries in the presence of the fields is the molecular point group $D_2 = \{E, C_2^x, C_2^y, C_2^z\}$, where E stands for the identity and C_2^i represents a rotation of π around the i-axis of the MFF, with $i = x, \quad y, \quad z$. The action of these operators on the Euler angles are summarized in Table I. The D_2-group has four irreducible representations.

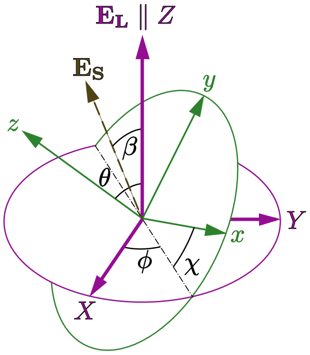

FIG. 1: Laboratory and molecular fixed coordinate frames and field configuration.

	Transformations		
Operation	ϕ	θ	χ
C_2^z	$\phi \to \phi$	$\theta \to \theta$	$\chi \to \chi - \pi$
C_2^y	$\phi \to \phi$	$\theta \to \pi - \theta$	$\chi \to -\chi$
C_2^x	$\phi \to \phi - \pi$	$\theta \to \pi - \theta$	$\chi \to \pi - \chi$
$\sigma_{XZ}^{\dagger}$	$\phi \to 2\pi - \phi$	$\theta \to \theta$	$\chi \to \pi - \chi$
$C_X(\pi)$	$\phi \to 2\pi - \phi$	$\theta \to \pi - \theta$	$\chi \to \pi + \chi$
$C_{\perp Z}^{\alpha}(\pi)$	$\phi \to 2\alpha - \phi$	$\theta \to \pi - \theta$	$\chi \to \chi + \pi$
$C_Z(\delta)$	$\phi \to \phi + \delta$	$\theta \to \theta$	$\chi \to \chi$

TABLE I: Action of the symmetry operations on the Euler angles. †The reflection can not be represented only by a rotation and the operation $y \to -y$ should be performed as well.

The Wang states, defined as

$$|JKMs\rangle^w = \frac{1}{\sqrt{2}}\left(|JKM\rangle + (-1)^s|J-KM\rangle\right),\ K>0$$
$$|J0M0\rangle^w = |J0M\rangle,\ K=0,$$

with $s=0$ and 1, form the basis of these irreducible representations, characterized by the parity of $J+s$ and K. The action of the elements of the D_2-group is $C_2^i|JKMs\rangle^w = (-1)^{\lambda_i}|JKMs\rangle^w$, with $i=x,y,z$ and $\lambda_x = J+K+s$, $\lambda_y = J+s$, and $\lambda_z = K$. The states $|JKM\rangle$ are the eigenfunctions of the field-free symmetric top rotor

$$|JKM\rangle = (-1)^{M-K}\sqrt{\frac{2J+1}{8\pi^2}}D^J_{-M,-K}(\Omega), \tag{5}$$

with $D^J_{M,K}(\Omega)$ being the Wigner matrix elements [43], J the total angular momentum, and K and M the projections of $\mathbf{J}$ on the MFF z-axis and on the LFF Z-axis, respectively. To be self-contained, the definition and main properties of the Wigner matrix elements are in Appendix A.

For a field-free asymmetric top rotor, J and M are good quantum numbers, whereas, in contrast to a symmetric rotor, K is not well defined. For each M-value, there are four irreducible representations that depend on the parity of $J+s$ and K. The eigenstates are degenerate with respect to M, and for a certain M and J, the corresponding eigenfunctions are linear combinations of Wang states $|JKMs\rangle^w$ with different K values.

Since an external field defines a preferred direction in space, the symmetries of the corresponding Hamiltonian are reduced compared to the field-free case. As a consequence, the total angular momentum J is not a good quantum number, and only for certain field configurations M remains as a good quantum number.

In the presence of a nonresonant laser field linearly polarized along the Z-axis, the symmetry operations of the Hamiltonian are the D_2 point group, a rotation of an arbitrary angle δ around the Z-axis $C_Z(\delta)$, a rotation of π around an axis perpendicular to the Z-axis tilted at an angle α with respect to the X-axis $C_{\perp Z}^{\alpha}(\pi)$, and the reflection in any plane including the Z-axis (this reflection is equivalent to first applying a twofold rotation around any axis in the XY-plane followed by the action of the operator C_2^x or C_2^y [34]). Only M remains a good quantum number, and the levels with $\pm M$ are degenerate. Thus, we have eight irreducible representations for each $|M|>0$, but due to the reflection at the plane there is a twofold degeneracy and they can be effectively reduced to four representations being characterized by the parity of K and $J+s$, as in the field-free Hamiltonian. For $M=0$, there are eight irreducible representations labeled by the parities of J, K and s.

When an asymmetric top rotor is exposed to a static electric field (parallel to the Z-axis) or to both fields in the parallel configuration, i.e., $\beta=0$, the symmetry operations are C_2^z from the D_2 point group, the rotation $C_Z(\delta)$, and the reflection in any plane including the Z-axis. In these two cases, M is still a good quantum number, and the states M and $-M$ are degenerate. For a certain $|M|$, the group has 4 irreducible representations characterized by the parity of K and the parity of s. Those representations with the same parity of K and $M>0$ are degenerate in energy. The symmetric top eigenfunctions (5), with defined parity of K, form a basis of this irreducible representation. For the $M=0$ case, these four representations are not energetically degenerate.

For non parallel fields, M ceases to be a good quantum number. If the two fields are perpendicular, i.e., the electric field is parallel to the X-axis and $\beta=\pi/2$, the Hamiltonian commutes with only three symmetry operations: C_2^z, a rotation of π around the X-axis $C_X(\pi)$, and the reflection σ_{XZ} on the XZ-plane where the fields are contained, as well as their combinations. Using the field-free symmetric rotor wave functions, we can construct a basis for σ_{XZ},

$$|JKMq\rangle^{\sigma} = \frac{1}{\sqrt{2}}\left(|JKM\rangle + (-1)^q|J-K-M\rangle\right)$$

with M and/or $K \neq 0$, and

$$|J000\rangle^{\sigma} = |J00\rangle$$

with $M = K = 0$, where $q = 0$ and 1, and $\sigma_{XZ}|JKMq\rangle^{\sigma} = (-1)^{M+K+q}|JKMq\rangle^{\sigma}$; and one for $C_X(\pi)$

$$|JKMp\rangle^{X} = \frac{1}{\sqrt{2}}(|JKM\rangle + (-1)^{p}|JK-M\rangle),$$

with $M \neq 0$, and

$$|JK00\rangle^{X} = |JK0\rangle,$$

with $M = 0$, where $p = 0$ and 1, and satisfying $C_X(\pi)|JKMp\rangle^{X} = (-1)^{J+p}|JKMp\rangle^{X}$. The group of all the symmetry operators, C_2^z, σ_{XZ} and $C_X(\pi)$, has eight different irreducible representations according to the parity of $M+K+q$, $J+p$ and K. A basis of these irreducible representations is

$$\begin{aligned} |JKMqp\rangle_{\frac{\pi}{2}} &= \frac{1}{2}(|JKM\rangle + (-1)^{q}|J-K-M\rangle \\ &\quad +(-1)^{p}|JK-M\rangle + (-1)^{p+q}|J-KM\rangle), \end{aligned}$$

with $M \neq 0$ and $K \neq 0$,

$$|J0M0p\rangle_{\frac{\pi}{2}} = \frac{1}{\sqrt{2}}(|J0M\rangle + (-1)^{p}|J0-M\rangle),$$

with $M \neq 0$ and $K = 0$

$$|JK0q0\rangle_{\frac{\pi}{2}} = \frac{1}{\sqrt{2}}(|JK0\rangle + (-1)^{q}|J-K0\rangle),$$

with $M = 0$ and $K \neq 0$ and

$$|J0000\rangle_{\frac{\pi}{2}} = |J00\rangle,$$

with $K = M = 0$, where $q = 0$ and 1, $p = 0$ and 1, and the parity of $M+K+q$, K and $J+p$ are preserved.

Finally, when the fields form an angle $0 < \beta < \pi/2$, the Hamiltonian is invariant under the reflection σ_{XZ} and the rotation C_2^z. We have, therefore, four irreducible representations depending on the parity of $M+K+q$ and of K, and the corresponding basis is $\{|JKMq\rangle^{\sigma}\}$.

For an asymmetric top rotor exposed to any of these field configurations, the field-dressed spectrum exhibits many avoided crossings between energetically adjacent states of the same symmetry. When the spectrum is analyzed as the strength of one of these fields is varied or the angle between them, these avoided crossings should be distinguished from the real crossings taking place between levels of different symmetry. Hence, we solve the Schrödinger equation, by expanding the rotational wave function in a basis that respects the symmetries of the corresponding Hamiltonian. As a consequence, the coefficients of these expansions fulfill the properties of the basis vectors of the corresponding irreducible representation. For computational reasons, we have cut the (in principle) infinite serie to a finite one including only those functions with $J \leq J_{\max}$, and for a certain J all $(2J+1)$-values of K, and, analogously, for M in the case $0 < \beta \leq \pi/2$. The size of the Hamiltonian matrix increases as $J_{\max}^3$ and $J_{\max}^2$ for the $0 < \beta \leq \pi/2$ and $\beta = 0$ configurations, respectively. In this study, we have used $J_{\max} = 24$, and the convergence is reached for the states analyzed here. Several matrix elements are presented in Appendix A.

The field-free states are labeled by the notation $J_{K_a,K_c}M$, where K_a and K_c are the values of K on the limiting symmetric top rotor prolate and oblate cases, respectively [47]. For reasons of addressability, we use this notation for the field-dressed states, even if J and/or M are not good quantum numbers. Thus, $J_{K_aK_c}M$ refers to the level that is adiabatically connected as I, E_S and/or β are modified with the field-free state $J_{K_aK_c}M$. The irreducible representation to which the states belong is also indicated. Analogously to a symmetric top molecule exposed to combined fields [35], the final labels of the states depend on the path followed on the parameters to reach a certain field configuration, i.e., monodromy is observed. Since each interaction breaks different symmetries of the field-free Hamiltonian, the order the fields are turned on determines the evolution of the field-dressed states. The complexity of the spectrum is characterized by the amount of genuine and avoided crossings among the states, the symmetry of the two levels determine the type of crossing that they may suffer as one of the field parameters (E_S, I or β) is varied, and, therefore, if the corresponding labels may or not be interchanged.

III. RESULTS

In this section, we illustrate the impact of the external fields on two asymmetric top molecules: fluorobenzene (C_6H_5F) and pyridazine ($C_4H_4N_2$). Their data are summarized in Table II, according to Refs. [48–52] and their structure is shown in Fig. 2. They are characterized by a different degree of asymmetry, the fluorobenzene is intermediate-prolate with $\kappa = -0.5879$, and the pyridazine is near-oblate with $\kappa = 0.8824$. The permanent dipole moment of pyridazine is around 2.5 times larger than in fluorobenzene. The asymmetry of the polarizability tensor is very similar for both systems, for fluorobenzene, $\alpha^{zx} = 4.298\text{Å}^3$ and $\alpha^{yx} = 3.848\text{Å}^3$, whereas for pyridazine $\alpha^{zx} = 4.51\text{Å}^3$ and $\alpha^{yx} = 4.45\text{Å}^3$. Since the rotational constants of pyridazine are larger than for fluorobenzene, for the same laser intensity, a weaker impact on the former should be expected. In the following, we carry out a study of the spectrum of these two systems as the parameters that characterize the field configurations, E_S, I or β, are modified. For the sake of simplicity, we analyze the energy, the orientation, the alignment and hybridization of the states which belong to the representation with K and $M+K+q$ even (if $\beta \neq \pi/2$), and $J+p$ even (if $\beta = \pi/2$). Note that they represent well the main physical features observed in the overall spectrum, and similar behavior and properties are therefore obtained for the other representations.

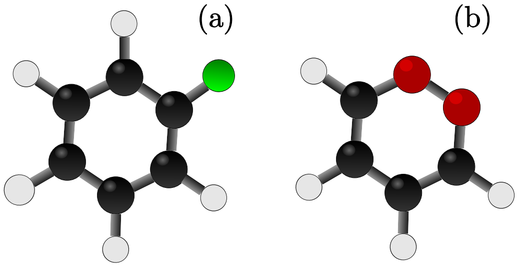

FIG. 2: Structure of the (a) fluorobenzene and (b) pyridazine molecules.

	Fluorobenzene	Pyridazine
B_x (MHz)	1716.916	3055.485
B_y (MHz)	2570.624	6048.613
B_z (MHz)	5663.72	6235.680
κ	-0.5879	0.8824
μ_z (D)	1.66	4.14
α_{xx} (Å^3)	7.141	5.84
α_{yy} (Å^3)	10.89	10.29
α_{zz} (Å^3)	11.439	10.35

TABLE II: Relevant data for fluorobenzene [48–50] and pyridazine [51, 52].

A. Impact of a linearly polarized laser field

The dynamics of the molecule in the presence of a linearly polarized laser field depends strongly on the anisotropy of the polarizability tensor. The interaction with the laser (4) exhibits several critical points. The minimum value $H_L = -I\alpha^{zx}/2\epsilon_0 c$ is reached for $\theta = 0$ or π and any value of χ. The interaction achieves three maxima at $\theta = \pi/2$ and $\chi = 0, \pi$ or 2π satisfying that $H_L = 0$, and two saddle points at $\theta = \pi/2$ and $\chi = \pi/2$ or $3\pi/2$ with $H_L = -I\alpha^{yx}/2\epsilon_0 c$. All of them are shown in Figs. 3(a) and (b), where H_L is plotted for $\chi = \pi/2$ and $0 \leq \theta \leq 2\pi$, and for $\theta = \pi/2$ and $0 \leq \chi \leq 2\pi$, respectively. The main difference between the two systems is that the values for H_L at the saddle point $\theta = \pi/2$ and $\chi = \pi/2$ is smaller for pyridazine compared to fluorobenzene, and the fact that the shape of H_L as a function of θ and for fixed χ is significantly flatter for the former. Taking into account that the rotational constants are much larger for pyradizine compared to fluorobenzene we observe that for the same laser intensity I, the pyridazine wave function is more widespread with respect to θ and χ than for fluorobenzene. While the minima are responsible for the molecular alignment, the maxima or saddle points correspond to an "antialigned" wave function, that is the dipole moment points perpendicular to the field direction.

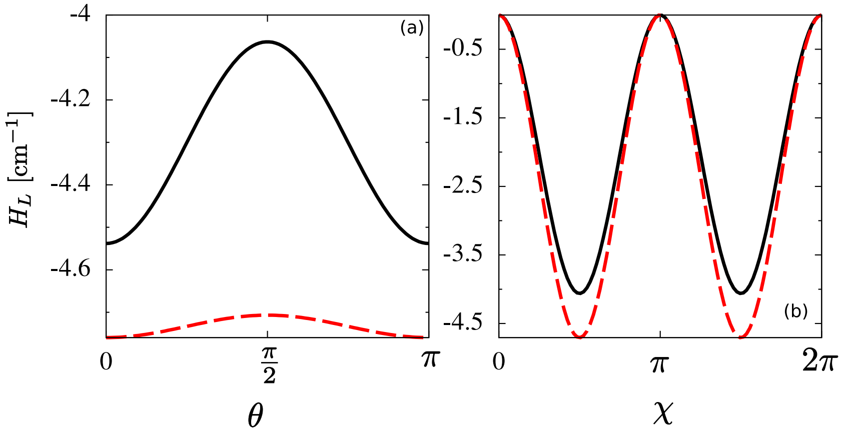

FIG. 3: Laser interaction term H_L, see eq. (4), in units of cm^{-1} with $I = 10^{11}$ Wcm^{-2}, for $\chi = \pi/2$ (a) and $\theta = \pi/2$ (b) for fluorobenzene (solid) and pyridazine (dash).

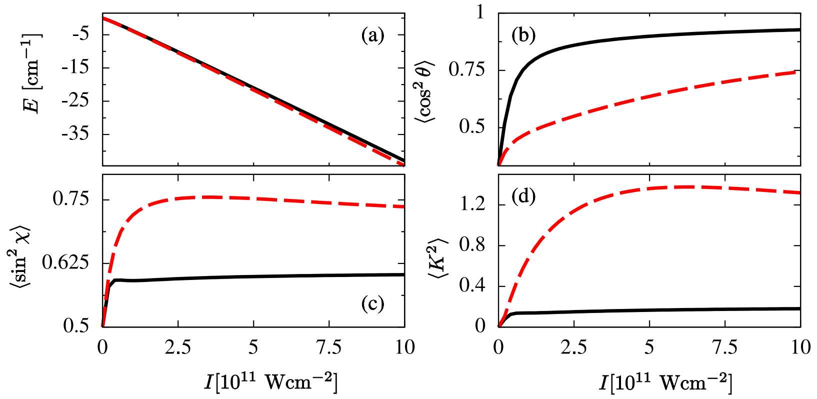

FIG. 4: Ground state energy (a), $\langle\cos^2\theta\rangle$ (b), $\langle\sin^2\chi\rangle$ (c), and $\langle K^2\rangle$ (d), as a function of the intensity of a linearly polarized laser field, for the fluorobenzene (solid) and pyridazine (dash) molecules.

To get a better physical insight into this interaction, we present its impact on the ground state energy, and the expectation values $\langle\cos^2\theta\rangle$, $\langle\sin^2\chi\rangle$, and $\langle K^2\rangle$ in Figs. 4(a), (b), (c), and (d), respectively. While, for both molecules, the energy as a function of I shows a similar decreasing behavior, their values being indistinguishable on the scale of Fig. 4(a), significant differences are observed for the other quantities. In the very strong laser field regime, the probability density of the fluorobenzene ground state tends to concentrate around the minima, and one should expect that $\langle\cos^2\theta\rangle \to 1$, and $\langle\sin^2\chi\rangle \to 0.5$ for very large intensities. This last relation holds because the χ-coordinate does not play any role in the absolute minima of H_L, and one concludes that the probability density should be uniformly distributed with respect to χ. Numerically we obtain that for the fluorobenzene ground state, $\langle\cos^2\theta\rangle$ increases until 0.76 for $I = 10^{11}$ Wcm^{-2}, decreasing thereafter, and $\langle\sin^2\chi\rangle$ reaches a plateau with a constant value 0.58 for $I \geq 4.2\cdot 10^{10}$ Wcm^{-2}. The barrier height of H_L as a function of θ for a certain value of χ, see Fig. 3(a), is around 9.2 times smaller for pyridazine than for fluorobenzene, and for the former, the rotational constants are larger, whereas the polarizability anisotropies α^{zx} and α^{yx} are of the same order for both molecules. Hence, compared to fluorobenzene, the pyridazine ground state wave function should be spatially stronger delocalize with respect to θ, and, therefore, less aligned for the same laser intensity. We obtain here $\langle\cos^2\theta\rangle = 0.49$ for $I = 10^{11}$ Wcm^{-2}. As a consequence, the spreading of the wave function for χ is not observed in pyridazine: $\langle\sin^2\chi\rangle$ shows a maximum of 0.75 for $I = 3\cdot 10^{11}$ Wcm^{-2} and slightly decreases with further increasing I. For the field-free ground state, we have $\langle K^2\rangle = 0$, and as I is increased $\langle K^2\rangle$ follows a similar evolution as $\langle\sin^2\chi\rangle$. For fluorobenzene, $\langle K^2\rangle$ achieves the value 0.14 for $I \approx 7.2\times 10^{10}$ Wcm^{-2}, followed by a plateau-like behavior around $\langle K^2\rangle \approx 0.18$ for larger intensities for fluorobenzene, while it keeps an increasing trend up to 1.38 for $I = 5.9\times 10^{11}$ Wcm^{-2} and decreasing smoothly afterwards for pyridazine. Let us emphasize that, for a field-free asymmetric rotor, K is not a good quantum number, and an eigenstate already shows a certain amount of K-mixing, but in the strong laser field regime, the second term of the laser interaction (4) should impact and enhance this K-mixing.

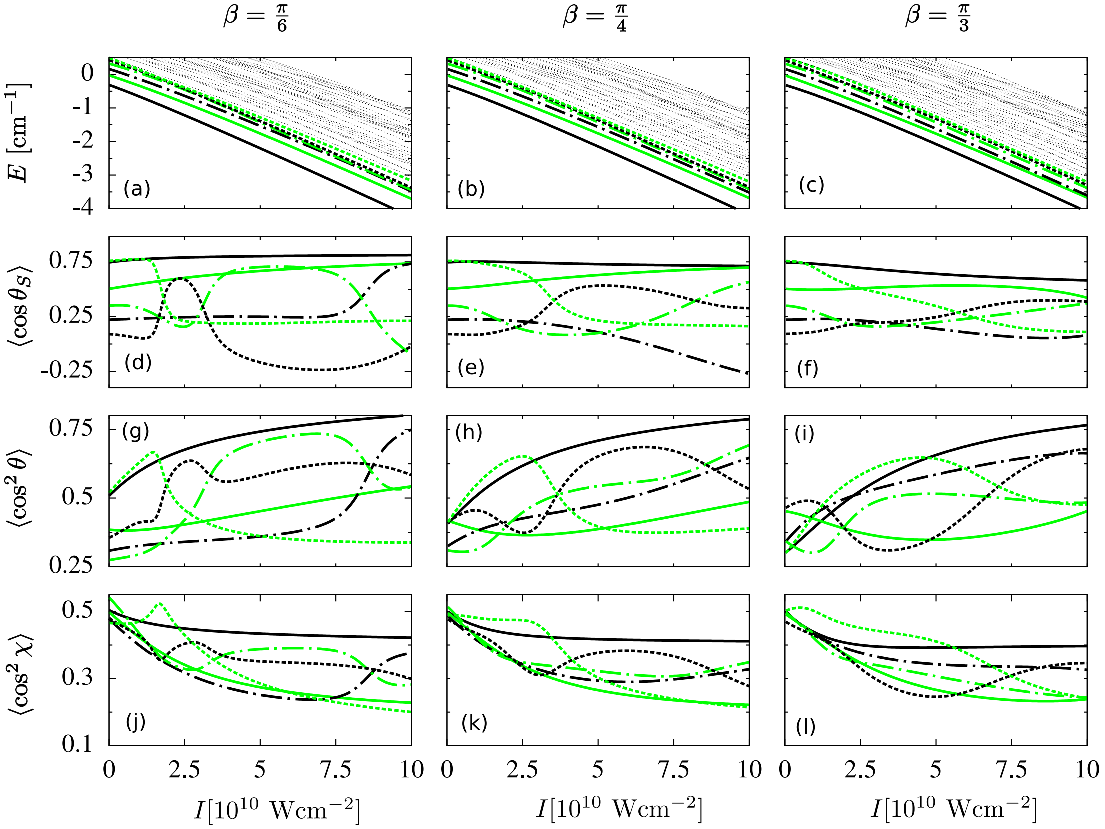

FIG. 5: (a)-(c) Energies and the expectation values (d)-(f) $\langle \cos\theta_S \rangle$, (g)-(i) $\langle \cos^2\theta \rangle$ and (j)-(l) $\langle \cos^2\chi \rangle$ for a constant field $E_S = 20$ kVcm^{-1} as a function of the intensity of the laser field for $\beta = \pi/6$, $\pi/4$ and $\pi/3$ for the first states with both $M + q + K$ and K even for fluorobenzene. The states are $0_{00}0$ (solid black), $1_{01}1$ (solid green), $1_{01}0$ (dash dotted black), $2_{02}2$ (dash dotted green), $2_{02}1$ (dash black) and $3_{03}2$ (dash green). The spectrum (a, b, c) contains also highly excited states (very thin lines).

B. Constant static electric field and increasing laser intensity

In the presence of an additional static field, the interaction is given by $H_S + H_L$, see eqs. (3) and (4), and the dynamics is significantly more complicated. The amount of extremal points of this potential and their character strongly depend on the field parameters as well as on the molecular polarizability and permanent dipole moment.

For fluorobenzene and pyridazine, we show in Figs. 5 and 6 the dependence of the energies (panels (a), (b), and (c)), expectation values $\langle \cos\theta_S \rangle$ (panels (d), (e), and (f)), $\langle \cos^2\theta \rangle$ (panels (g), (h), and (i)), and $\langle \cos^2\chi \rangle$ (panels (j), (k), and (l)), as functions of the laser intensity for a constant electric field $E_S = 20$ kVcm^{-1}, and $\beta = \pi/6$, $\pi/4$ and $\pi/3$, respectively. For the sake of simplicity and without loosing generality, we restrict our analysis to the energetically lowest-lying six states for the irreducible representations with both K and $M + K + q$ being even, which are the levels $J_{K_a,K_c}M = 0_{00}0$, $1_{01}0$, $1_{01}1$, $2_{02}1$, $2_{02}2$ and $3_{03}2$ for fluorobenzene, and $J_{K_a,K_c}M = 0_{00}0$, $1_{01}0$, $1_{01}1$, $2_{02}1$, $2_{02}2$, and $2_{21}2$, for pyridazine. To illustrate the complexity of the spectrum, we have included in the energy panels highly excited levels with the same symmetry (very thin lines). The adiabatic following has been done by increasing first the strength of the static electric field up to 20 kVcm^{-1}, the static field being tilted by an angle β with respect to the Z-axis. This is done for $I = 0$ and yields the labeling of the states in the presence of the static field. Thereafter, the laser intensity is increased. For both molecular systems, these levels are high-field-seekers, and their energies decrease as I is increased. For a given laser intensity, the lowering in energy (compared to the field-free value) increases with decreasing angle between both fields. Since all the states included in these figures possess the same symmetry, we encounter exclusively avoided crossings of energetically adjacent states. We have assumed that the avoided crossings are traversed adiabatically as I is increased (according to Landau-Zener transition theory), and consequently the character of the involved states is interchanged. These avoided crossings, which are not distinguishable on the energy scale panels (a)-(c) in Figs. 5 and 6, strongly affect the orientation and alignment features of these levels.

Let us start analyzing the results for fluorobenzene in Fig. 5. The orientation of the corresponding wave functions is illustrated by the expectation value $\langle\cos\theta_S\rangle$, with θ_S being the angle between the static electric field and the molecular fixed z-axis, which coincides with the direction of the permanent dipole moment. Only the states $0_{00}0$ and $3_{03}2$ present a significant orientation with respect to the static electric field direction, that is reduced as β is increased. The ground state satisfies $\langle\cos\theta_S\rangle > 0.70$ for the three β values, and it has a plateau like behavior, with a minor positive or negative slope as I is increased. The numerous avoided crossings have significant impact on the other levels especially for $\beta = \pi/6$ and $\pi/4$, and the underlying states might evolve from a strongly oriented configuration into a weakly oriented or antioriented one. As an example, the state $3_{03}2$ after suffering for $I \approx 1.7 \cdot 10^{10}$ Wcm^{-2} an avoided crossing with the non-oriented $2_{02}1$ state looses its strong orientation. By further increasing I the $2_{02}1$ level suffers another avoided crossing, which provokes a local maximum in $\langle\cos\theta_S\rangle$ for $I \approx 2.4 \cdot 10^{10}$ Wcm^{-2}. Since for $\beta = \pi/3$ the width of all the avoided crossings is larger for all the levels, the orientation shows a smooth evolution as I is varied. A nonresonant linearly polarized laser field provokes the alignment of the wave function along the Z-axis, i.e., $\left\langle\cos^2\theta\right\rangle$ tends to increase and ultimately approach the value 1 as I is increased (Fig. 5(g, h, i)). This process competes now with the orientation due to the static field. Only the ground state alignment keeps an increasing trend as I is enhanced, and for the given three configurations $\left\langle\cos^2\theta\right\rangle > 0.75$ for $I = 10^{11}$ Wcm^{-2}. An additional electric field at an angle $\beta = \pi/6$ or $\pi/4$ favors the alignment and $\left\langle\cos^2\theta\right\rangle$ is larger than without static field, see Fig. 4(b), whereas as the angle between the fields is augmented the values achieved for $\left\langle\cos^2\theta\right\rangle$ come closer to those of Fig. 4(b). The level $1_{01}1$ does not achieve a large alignment, and for $\beta = \pi/4$, $\left\langle\cos^2\theta\right\rangle$ exhibits a broad well that for $\beta = \pi/3$ is even wider since the coupling between the states changes. Around the avoided crossings, the wave function of the involved states alternate regions of significant alignment with other characterized by broad distribution as the laser intensity is varied, e. g. see the aligment of the states $3_{03}2$ and $2_{02}1$ for $I \approx 1.7 \cdot 10^{10}$ and $3.5 \cdot 10^{10}$ Wcm^{-2} in Fig. 5 (g) and (h), respectively. The impact of the avoided crossings is also noticeable for $\beta = \pi/3$. The behavior of $\left\langle\cos^2\chi\right\rangle$ strongly depends on the considered level. Since the molecules exhibit a strong orientation with the electric field, the contribution in χ should be to increase the term $\left\langle\sin^2\chi\right\rangle$ which will give rise to a decrease of the energy. For the

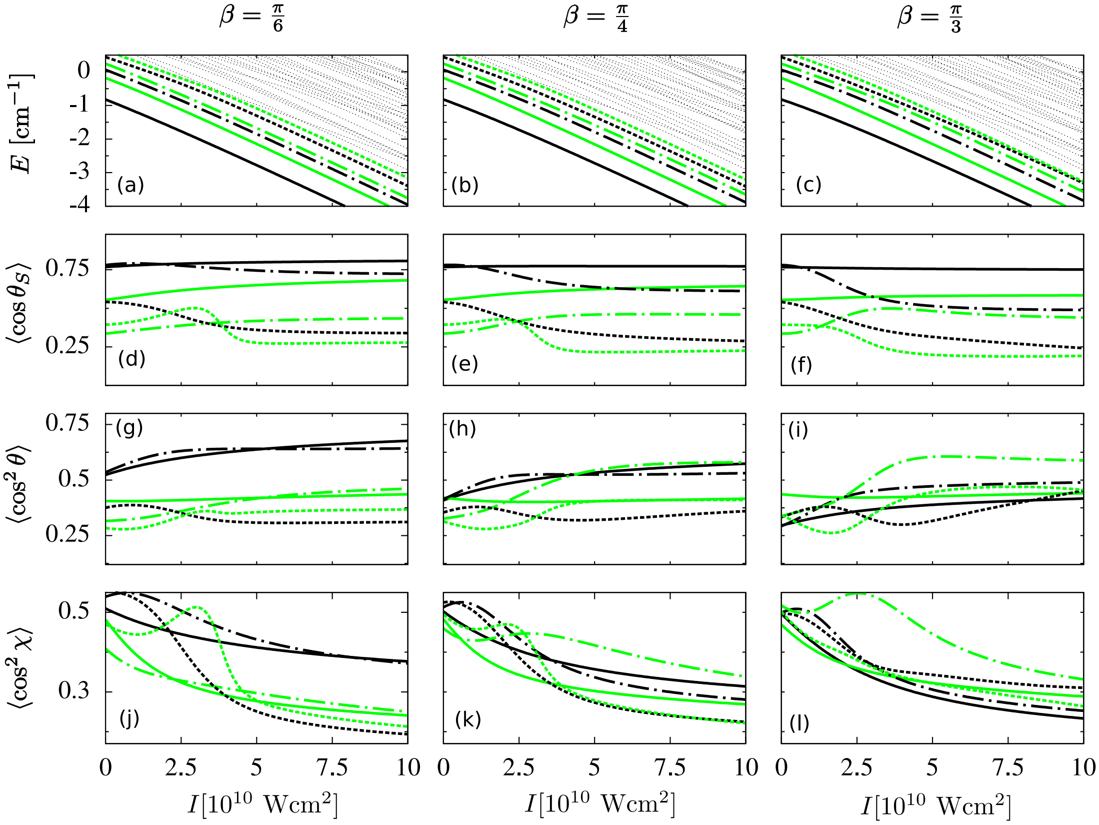

FIG. 6: (a)-(c) Energies and the expectation values (d)-(f) $\langle\cos\theta_S\rangle$, (g)-(i) $\langle\cos^2\theta\rangle$ and (j)-(l) $\langle\cos^2\chi\rangle$ for a constant field $E_S = 20$ kVcm^{-1} as a function of the intensity of the laser field for $\beta = \pi/6$, $\pi/4$ and $\pi/3$ for the first states with both $M + q + K$ and K even for pyridazine. The states are $0_{00}0$ (solid black), $1_{01}1$ (solid green), $2_{02}2$ (dash dotted black), $1_{01}0$ (dash dotted green), $2_{02}1$ (dash black) and $2_{21}2$ (dash green). The spectrum (a, b, c) contains also highly excited states (very thin lines).

states $0_{00}0$ and $1_{01}1$, $\langle\cos^2\chi\rangle$ decreases as I is increased, and for both states there exists some region where $\langle\cos^2\chi\rangle$ keeps a smooth behavior. For the other states, this expectation value is also affected by the presence of avoided crossings, and $\langle\cos^2\chi\rangle$ alternates between increasing and decreasing behavior as a function of the laser intensity. Since the pyridazine possesses a larger permanent dipole moment than fluorobenzene, the impact of the static field is larger, and also dominates the dynamics, see Fig. 6. For the ground state and first excited one, $\langle\cos\theta_S\rangle$ is only weakly affected by the laser field, for the former $\langle\cos\theta_S\rangle \approx 0.75$ independently of I and β, while for the $1_{01}1$ level $\langle\cos\theta_S\rangle > 0.5$. The other levels present a right-way orientation, that can be converted from a strong to a mild one when an avoided crossing is encountered. Regarding the alignment, for most of the states $\langle\cos^2\theta\rangle$ shows a smooth behavior as I is enhanced for the three values of β. The impact of the avoided crossings on this expectation value is not very pronounced because most of the states show a weak alignment with a similar value of $\langle\cos^2\theta\rangle$. Analogously to fluorobenzene, the ground state has a larger alignment for $\beta = \pi/6$ and $\pi/4$ than in the absence of the static field, while for $\beta = \pi/3$ other states are found with larger alignment. For stronger fields, $\langle\cos^2\chi\rangle$ monotonically decreases as I is enhanced for all the states, and the slope is more pronounced compared to fluorobenzene.

C. Constant laser intensity and increasing electric field strength

The pendular limit of an asymmetric top molecule in the presence of a strong electrostatic field was investigated by Kanya and Ohshima [34] using a power series expansion in μE_S. Their analytical expression for the energy, which neglects the contribution of terms in powers equal or smaller than $(\mu E_S)^{-1/2}$ (see eq. (26) in Ref. 34) allowed us for a straightforward comparison to our numerical calculations. For $E_S = 100$ kVcm^{-1}, the energy and orientation cosine of the ground state agree within 0.05% and 0.025% for fluorobenzene and 0.04% and 0.019% pyridazine, respectively. Note that for highly excited states these relative errors increase.

For a constant laser field $I = 10^{10}$ Wcm^{-2}, we now investigate the impact of increasing static field strength for three different configurations. Again, we consider the energetically lowest-lying six states with the irreducible representation for K and $M + K + q$ being even. These levels have been adiabatically followed as the laser intensity is raised from $I = 0$ to 10^{10} Wcm^{-2} for $E_S = 0$, we label them, and finally the electrostatic field is turned on forming an angle β and its strength is increased. Thus, for both molecules the levels are $0_{00}0$, $1_{01}0$, $1_{01}1$, $2_{02}0$, $2_{02}1$, and $2_{02}2$. For fluorobenzene and pyridazine, we present in Figs. 7 and 8, the evolution of the energies (panels (a), (b), and (c)), $\langle\cos\theta_S\rangle$ (panels (d), (e), and (f)), and $\langle\cos^2\theta\rangle$ (panels (g), (h), and (i)), as E_S is increased, for $I = 10^{10}$ Wcm^{-2}, and

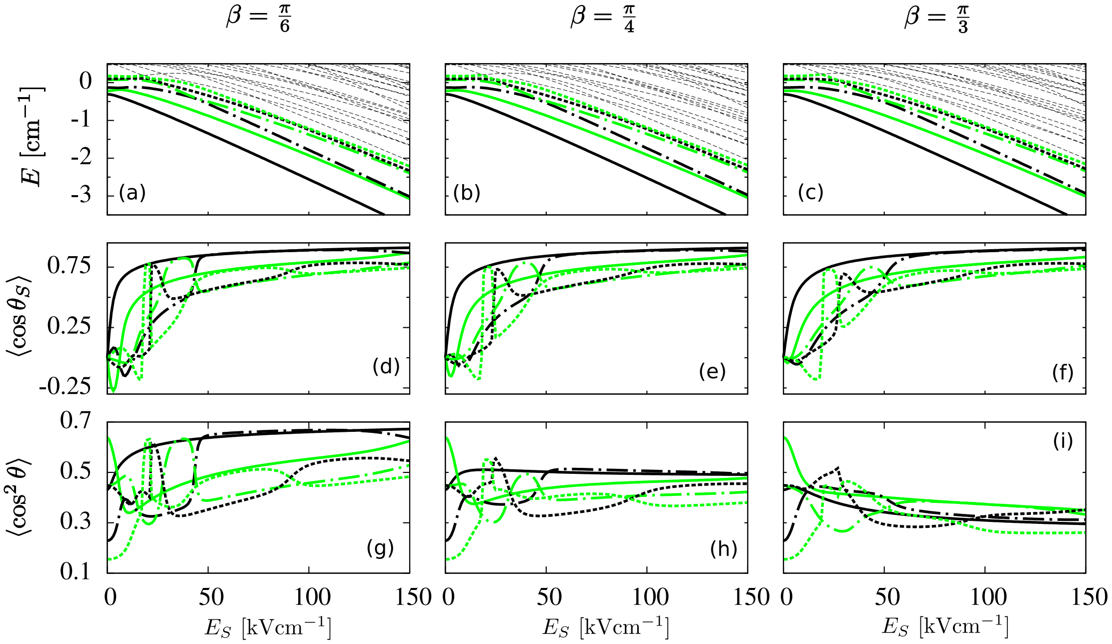

FIG. 7: (a)-(c) Energies and the expectation values (d)-(f) $\langle\cos\theta_S\rangle$, (g)-(i) $\langle\cos^2\theta\rangle$ for a constant $I = 10^{10}$ Wcm^{-2} as a function of the strength of the static field for $\beta = \pi/6$, $\pi/4$ and $\pi/3$ for the energetically lowest states with both $M+q+K$ and K even for fluorobenzene. The states are $0_{00}0$ (solid black), $1_{01}0$ (solid green), $1_{01}1$ (dash dotted black), $2_{02}0$ (dash dotted green), $2_{02}1$ (dash black) and $2_{02}2$ (dash green). The spectrum (a, b, c) contains also highly excited states (very thin lines).

$\beta = \pi/6, \pi/4$ and $\pi/3$, respectively. We remark that for such a weak laser intensity $I = 10^{10}$ Wcm^{-2} a static electric field of $E_S \geq 17.08$ and 7.26 kVcm^{-1} for fluorobenzene and pyridazine, respectively, provides the larger contribution to the external field Hamiltonian $H_S + H_L$. If the interaction with the static field is dominant and much larger than the laser one, i.e., $E_s\mu \gg I\alpha^{ix}/2\epsilon_0 c$ with $i = y$ or z, the absolute minima of the potential $H_S + H_L$ are at (ϕ, β, χ), with $\phi \to 0, 2\pi$ and $\chi \to \pi/2, 3\pi/2$. Thus, the wave function will be oriented toward the electric field direction with $\langle\cos^2\theta\rangle \to \cos^2\beta$ and $\langle\cos\theta_S\rangle \to 1$. However, these extremal points do not provoke any effect on the χ coordinate, because in the strong static field regime, the variation of $H_S + H_L$ as a function of χ represents a very shallow minimum and does not give rise to a localization of the wave function.

In the weak field regime there are, for both molecules, several levels in addition to the ground state that are high-field seekers, and remaining levels are for low values of E_S low-field seekers. These levels present a mild wrong-way orientation with $\langle\cos\theta_S\rangle < 0$. Since in this regime the slope of the variation of the energy with E_S might be positive or negative, this favors the presence of sharp avoided crossings. As a consequence, the orientation of a pair of levels involved in an avoided crossings, i.e., $\langle\cos\theta_S\rangle$, suffers drastic variations over tiny ranges of the field strength. As the field strength is increased, we encounter the pendular regime: all the states are high-field-seekers, and they are strongly oriented along the static field direction. Indeed, for $E_S = 100$ kVcm^{-1}, we have that $\langle\cos\theta_S\rangle > 0.60$ and 0.70 for the considered fluorobenzene and pyridazine levels, respectively. In this regime, we still encounter avoided crossings but they are much wider. Due to the competition between both fields, these states do not achieve a significant alignment, see panels (g)-(i) in Fig. 7 and 8. We observe that $\langle\cos^2\theta\rangle$ approaches $\cos^2\beta$ in the strong field regime.

D. Orientation and 2-D alignment by means of perpendicular fields

External fields provide a tool to control the molecular dynamics: specifically it has been shown that an elliptically polarized laser allows for *3-D alignment* of asymmetric molecules, i.e., the system is aligned in all spatial directions [26, 28, 53, 54]. We show here that the combination of an electrostatic field with the linearly polarized laser gives rise to orientation in one direction and alignment in the other two. We hereby focus on the case $\beta = \pi/2$. In the strong static field regime, we have $\theta \to \pi/2$ and $\phi \to 0$, whereas, in order to decrease the energy the term $\sin^2\chi$ in the laser Hamiltonian (4) should increase and approach one, i.e., $\chi \to \pi/2, 3\pi/2$. Then, the molecule will be fixed in space, and the wave function should be concentrated in the proximity of $\theta \sim \pi/2$, $\chi \sim \pi/2$, $3\pi/2$ and $\phi \sim 0$, 2π. To demonstrate this behavior we have computed the 1D probability density distribution in each one of the three Euler angles by integrating the square of the wave function in the other two angles. In Fig. 9(a), (b), and (c), these probability density distributions $\Theta(\theta)\sin\theta$, $\Phi(\phi)$ and $\Xi(\chi)$ are plotted as a function of θ, ϕ and χ, respectively, for the ground state of pyridazine interacting with the orthogonal fields for different strengths. The probability density distributions

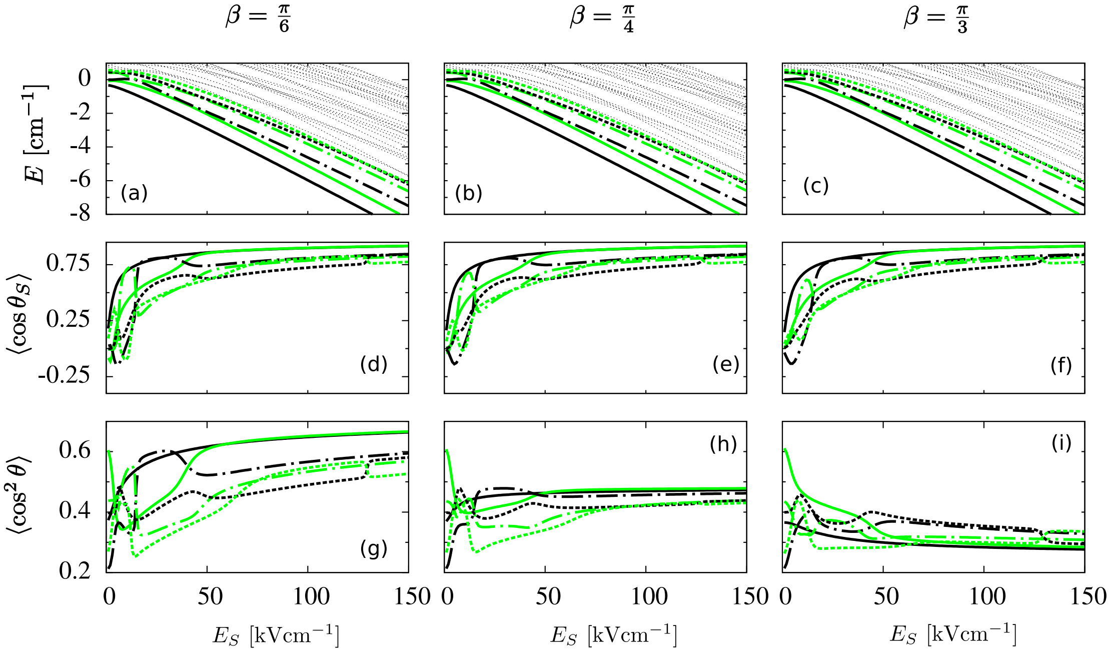

FIG. 8: Same as Fig. 7 but for pyridazine.

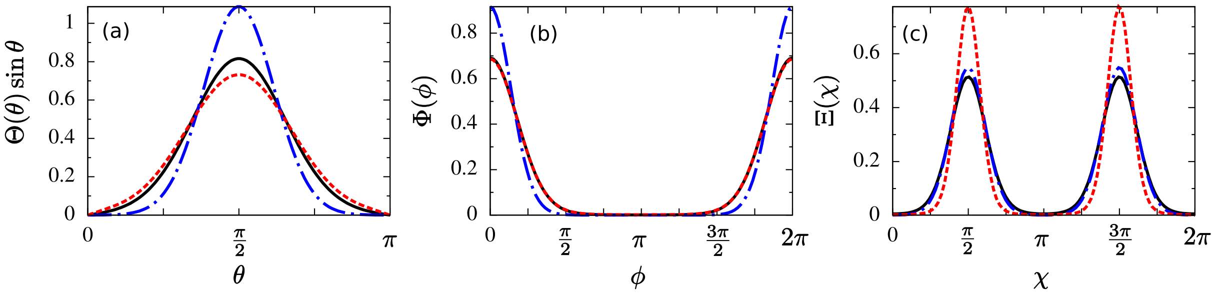

FIG. 9: One dimensional probability density distribution in each Euler angle for the ground state of pyridazine for $E_S = 20$ kVcm^{-1} and $I = 10^{11}$ Wcm^{-2} (solid), $E_S = 50$ kVcm^{-1} and $I = 10^{11}$ Wcm^{-2} (dash dotted), $E_S = 20$ kVcm^{-1} and $I = 5 \cdot 10^{11}$ Wcm^{-2} (dash).

for $E_S = 20$ kVcm^{-1} and $I = 10^{11}$ Wcm^{-2} show the expected behavior, and this state presents a significant orientation along the X-axis of the LFF with $\langle\cos\theta_S\rangle = 0.749$ and $\langle\cos^2\theta\rangle = 0.191$, whereas the alignment in the other two Euler angles is also pronounced and we get $\langle\cos^2\chi\rangle = 0.143$ and $\langle\cos^2\phi\rangle = 0.661$. A larger orientation is achieved if the static field strength is enhanced to $E_S = 50$ kVcm^{-1} keeping the same laser intensity: $\langle\cos\theta_S\rangle = 0.849$ and $\langle\cos^2\theta\rangle = 0.118$, for the distribution in χ and ϕ and we find $\langle\cos^2\chi\rangle = 0.122$ and $\langle\cos\phi\rangle = 0.723$, respectively. An opposite effect has the enhancement of the laser intensity to $I = 5 \cdot 10^{11}$ Wcm^{-2} and keeping $E_S = 20$ kVcm^{-1}. The orientation in θ is slightly reduced $\langle\cos\theta_S\rangle = 0.729$ and $\langle\cos^2\theta\rangle = 0.222$, but $\langle\cos^2\phi\rangle$ increases only to 0.682, that is, the laser does not affect the azimuthal angle and in Fig. 9(b) the distribution $\Phi(\phi)$ is indistinguishable compared to the corresponding one for $E_S = 20$ kVcm^{-1} and $I = 10^{11}$ Wcm^{-2}. The alignment with respect to χ becomes stronger $\langle\cos^2\chi\rangle = 0.075$. Of course, one should keep in mind that this effect is very sensitive to the fields strengths and their configuration, as well as and the molecular parameters, i. e., the permanent dipole moment, polarizability anisotropies and rotational constants. For fluorobenzene, a similar phenomenon could be found, but the wave function shows a slightly less pronounced orientation and alignment. If the fields are not perpendicular, the competition between both interactions will reduce the alignment achieved in the ϕ and χ angles.

E. Influence of the inclination of the fields

The inclination of the fields plays an essential role on their impact on the rotational dynamics of the system, and as already discussed, the symmetries are drastically modified as β is varied. Indeed, β is another parameter in the Hamiltonian that enriches the physical phenomena observed, and its variation can provoke the appearance of avoided crossings between energetically adjacent states of the same symmetry. For pyridazine, we represent in Figs. 10 (a) the energy, (b) $\langle\cos\theta_S\rangle$, (c) $\langle\cos^2\theta\rangle$, and (d) $\langle M^2\rangle$, as a function of β with $E_S = 20$ kVcm^{-1} and $I = 10^{11}$ Wcm^{-2}, for the previous set of states with K and $M + K + q$ even and following the same labeling as in Sec. III B. For these field strengths, the static electric field interaction dominates over the laser field interaction, similar to Fig. 8. In general, the energies show a smooth behavior as β is varied, and depending on the state they exhibit an increasing or decreasing trend, see Fig. 10(a), e.g., the ground state energy increases from -5 cm^{-1} to -4.6 cm^{-1} from $\beta = 0$ to $\pi/2$, respectively. The energy gap between the first four states is large enough to prevent the presence of avoided crossings among them, the first avoided crossing being between the fourth and fifth excited states, $2_{02}1$ and $2_{21}2$, for $\beta \approx 1.096$ (close to $3\pi/8$). Regarding the orientation and alignment along the electric and laser fields directions, respectively, different behaviors are observed. The ground state keeps a significant and approximately constant orientation with $\langle\cos\theta_S\rangle > 0.75$ for any value of β, as the electric field is rotated away from the Z-axis the ground state probability density follows this field. In contrast to this, since the laser interaction is not dominant, its alignment is drastically reduced from $\langle\cos^2\theta\rangle \approx 0.75$ to 0.22 when β increases from 0 to $\pi/2$. For any field configuration, the $1_{01}1$ level shows a moderate orientation and alignment with a plateau-like behavior for $\langle\cos\theta_S\rangle$ and $\langle\cos^2\theta\rangle$. Compared to the ground state, the $2_{02}2$ level presents a similar orientation and alignment for $\beta = 0$, but a very different evolution of these features as β is varied, and for $\beta = \pi/2$, it keeps a moderate alignment and a weak orientation. For parallel fields, M is a good quantum number, and a non-parallel configuration allows the interaction and mixing between states with different field-free M-value. This phenomenon is illustrated by means of the expectation value $\langle M^2\rangle$ in Fig. 10(d). As the angle β is increased, the evolution of $\langle M^2\rangle$ strongly depends on the character of the corresponding level. For the ground state, $\langle M^2\rangle$ increases as β is enhanced, and for $\beta = \pi/2$, it reads $\langle M^2\rangle = 0.746$. The $\langle M^2\rangle$ value of the $1_{01}1$ level is close to 1 for $\beta \leq \pi/8$, but for larger values of β decreases to 0.6 for $\beta = \pi/2$. In contrast, for the other

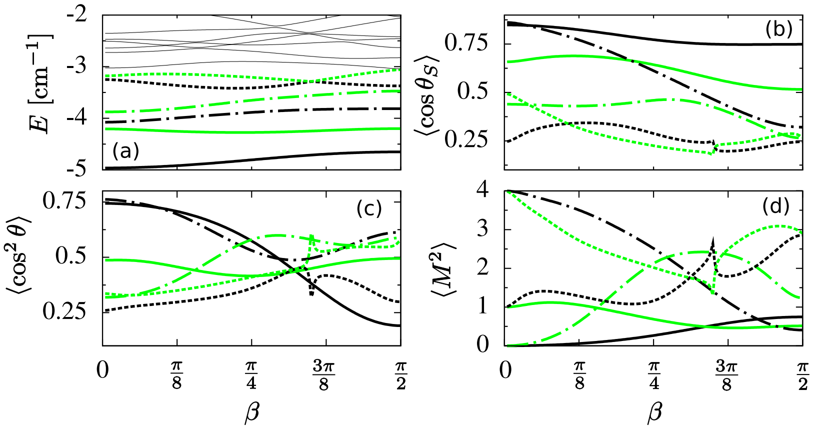

FIG. 10: (a) Energies and expectation values (b) $\langle\cos\theta_S\rangle$, (c) $\langle\cos^2\theta\rangle$ and (d) $\langle M^2\rangle$ for pyridazine in the presence of a static field $E_S = 20$ kVcm^{-1} and a laser field $I = 10^{11}$ Wcm^{-2} as a function of β for the energetically lowest states with both $M+q+K$ an K even. The states are $0_{00}0$ (solid black), $1_{01}1$ (solid green), $2_{02}2$ (dash dotted black), $1_{01}0$ (dash dotted green), $2_{02}1$ (dash black) and $2_{21}2$ (dash green).

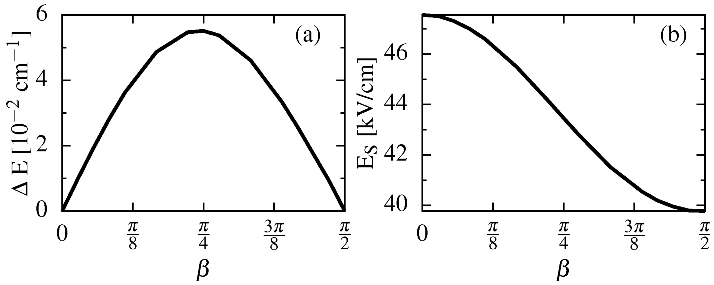

FIG. 11: Width ΔE (a) and electrostatic field strength E_S (b) at the avoided crossing taking place between the states $2_{02}0$ and $2_{02}1$ for pyridazine, for $I = 10^{10}$ Wcm^{-2} and different inclination angles β.

analyzed level with $M = 1$, $2_{02}1$, the interaction with states with larger M is dominant for $\beta > \pi/4$, and $\langle M^2\rangle = 3$ for $\beta = \pi/2$. For the considered $M = 2$ levels, $2_{02}2$ and $2_{21}2$, the mixing with states with lower M is dominant, and $\langle M^2\rangle$ is smaller than in the parallel configuration, e.g., for the $2_{02}2$ level and $\beta = \pi/2$, we have $\langle M^2\rangle = 0.4063$.

With varying inclination angle β between both fields the avoided crossings leave their fingerprints in the relevant observable. For pyridazine, the states $2_{02}0$ and $2_{02}1$ belong to different irreducible representations for $\beta = 0$ and $\pi/2$, and to the same one for $0 < \beta < \pi/2$. (Note that the labeling of the states has been done in the same way as in Fig. 8). For non collinear fields, they suffer an avoided crossing which we have traced for $I = 10^{10}$ Wcm^{-2} and different values of β in Fig. 11. The results for the minimal energetical width $\Delta E = |E_{2_{02}0} - E_{2_{02}1}|$ and the electrostatic field strength at which this minimum appears are presented in Figs. 11(a) and (b), respectively, as the angle β is varied. For perpendicular fields, the levels suffer a real crossing and are accidently degenerate $\Delta E = 0$ for $I = 10^{10}$ Wcm^{-2} and $E_S = 39.78$ kVcm^{-1}, whereas for $\beta = 0$, they possess a different magnetic quantum number M and exhibit a symmetry-related crossing but now for $E_S = 47.55$ kVcm^{-1}. As we see in panel (a), ΔE increases till it reaches the maximal value of $5.33\cdot10^{-2}$ cm^{-1} for $\beta = \pi/4$, decreasing afterwards to 0 for $\beta = \pi/2$. The static field strength at which the avoided crossing takes places, see panel (b), decreases monotonously as β increases. Indeed, the variation of E_s with β is well-matched by the following function $3.88\cos(2.06\beta) + 43.67$, and it is reduced by 7.74 kVcm^{-1} when β goes from 0 to $\pi/2$.

IV. CONCLUSIONS

In this work, we have investigated the impact of a combination of an electrostatic and a nonresonant linearly polarized laser field on the rotational spectrum of asymmetric top molecules. This study has been performed in the framework of the Born-Oppenheimer approximation considering that the vibrational and electronic dynamics are not affected by the external fields. Our analysis is restricted to a rigid rotor description of molecules having their permanent dipole moment parallel to one axis of inertia, and the polarizability tensor is diagonal in the basis formed by the principal axis of inertia. We have analyzed the symmetries and irreducible representations of the Hamiltonian for the different field configurations. Numerically, each irreducible representation has been treated independently, by expanding the wave function in a basis respecting the corresponding symmetries. This procedure allows us to distinguish the avoided crossings from genuine ones involving states of the same and different symmetry, respectively. The presence of the avoided crossings in the field-dressed spectrum affects the directional properties of the molecule, they might significantly alter the spectroscopy as well as the sterodynamic of the system. The labeling of a certain state and the passage through the avoided crossing that it suffers depend on the way the symmetries are broken, i.e., on the temporal sequence followed to turn on the fields, which should be taken into account to determine the adiabaticity of a certain process.

The richness and variety of the resulting field-dressed rotational dynamics have been illustrated by analyzing the energetic shifts, as well as the orientation, alignment and the hybridization of the angular motion. As prototype example we have investigated the fluorobenzene and pyridazine molecules. For three field configurations, the evolution of a certain set of states belonging to a certain symmetry has been analyzed with varying electrostatic field strength or laser intensity. Different types of behavior were observed, depending on the dominant field interaction as well as on the considered molecular system, through its rotational constant, dipole moment and polarizability tensor. Due to the competition between both interactions, the features of the rotational spectrum are significantly changed as the field parameters are modified. In the strong laser field regime, the presence of an intense electric field reduces the orientation of the ground state, especially as β is rotated from zero to larger values, and highly excited levels only present a very weak alignment. Whereas, if the electrostatic field is dominant the states are oriented along its direction, and they only present a mild alignment along the Z-axis in the LFF. We have shown that a proper combination of non-collinear fields gives rise to a strong orientation along the static field direction together with a 2D-alignment on the other two axis of the molecule. In particular for $\beta = \pi/2$, the molecular plane is fixed onto the XY-plane of the LFF, and the orientation is along the X axis. Finally, we have also investigated the role played by the inclination angle of the fields β, by analyzing the spectral properties of several states, the loss of the azimuthal symmetry has been quantified by the expectation value $\langle M^2 \rangle$, which is a conserved magnitude for parallel fields. An avoided crossing between two states has been traced as β is modified, the electrostatic field strength at which it takes places varies within a few kVcm^{-1}, and the corresponding energetical width will allow us to compute the adiabaticity of the crossing once the variation of the field strength is known. A natural extension to this work would be to consider other molecular systems, especially different conformers of the same molecule, looking for specific phenomena that might help to distinguish between the molecules.

Acknowledgments

Financial support by the Spanish project FIS2008-02380 (MICINN) as well as the Grants FQM-2445 and FQM-4643 (Junta de Andalucía) is gratefully appreciated. J.J.O. and R.G.F. belong to the Andalusian research group FQM-207. J.J.O. acknowledges the support of ME under the program FPU. We thank J. Küpper for fruitful discussions.

Appendix A: Wigner and Hamiltonian matrix elements

The field-free eigenstates of a symmetric top molecule, see eq. (5), are proportional to the Wigner matrix elements, $D^J_{M,K}(\Omega)$, which are defined as

$$D^J_{M,K}(\Omega) = e^{-iM\phi} d^J_{M,K}(\theta) e^{-iK\chi}, \tag{A1}$$

where $d^J_{M,K}(\theta)$ are the reduced Wigner matrix elements [43]. To evaluate the matrix elements of the Hamiltonian, we have used the following properties of the Wigner matrix, the complex conjugate

$$D^{J\dagger}_{M,K}(\Omega) = (-1)^{M-K} D^J_{-M,-K}(\Omega), \tag{A2}$$

the relation between the Wigner reduced matrix elements reads

$$\begin{aligned} d^j_{m',m}(\theta) &= (-1)^{m-m'} d^j_{m,m'}(\theta) & \text{(A3)}\\ d^j_{m',m}(\theta) &= (-1)^{m'-m} d^j_{-m',-m}(\theta) & \text{(A4)}\\ d^j_{m',m}(\theta) &= d^j_{m,m'}(-\theta) & \text{(A5)} \end{aligned}$$

and the integral of the triple product of Wigner matrices

$$\begin{aligned} \int d\Omega D^{J}_{-K,-M}(\Omega) D^{J_1}_{K_1,M_1}(\Omega) D^{J_2}_{K_2,M_2}(\Omega) = \\ = 8\pi^2 \begin{pmatrix} J_1 & J_2 & J \\ M_1 & M_2 & -M \end{pmatrix} \begin{pmatrix} J_1 & J_2 & J \\ K_1 & K_2 & -K \end{pmatrix}. \end{aligned} \tag{A6}$$

where $\begin{pmatrix} j_1 & j_2 & j_3 \\ m_1 & m_2 & m_3 \end{pmatrix}$ are the *3J Symbols*.

For completeness, we provide the non-zero matrix elements appearing in the evaluation of the full Hamiltonian. For the field-free Hamiltonian H_r (2), we have

$$\begin{aligned} \langle J'K'M'|H_r|JKM\rangle &= (AJ(J+1) + CK^2)\delta_{J',J}\delta_{K',K}\delta_{M',M} \\ &+ B\sqrt{J(J+1) - K(K+1)}\sqrt{J(J+1) - (K+1)(K+2)}\delta_{J',J}\delta_{K+2,K}\delta_{M',M}, \end{aligned}$$

where A, B and C are defined as $A = (B_x + B_y)/2$, $\quad B = (B_x - B_y)/4$, $\quad$ and $\quad C = (2B_z - B_x - B_y)/2$ [55]. The Stark interaction H_S (3) rewritten in terms of Wigner matrix elements, is given by

$$H_S = -\mu E_S \cos\theta_S = -\mu E_S h_S = -\mu E_S \left(\cos\beta D^1_{00}(\Omega) + \sin\beta \sqrt{\frac{1}{2}}(D^1_{-1,0}(\Omega) - D^1_{10}(\Omega)) \right), \tag{A7}$$

Thus, the non-zero matrix elements are

$$\begin{aligned} \langle JKM|h_S|JKM\rangle &= \frac{MK}{J(J+1)}\cos\beta \\ \langle JKM+1|h_S|JKM\rangle &= \frac{K\sin\beta}{2J(J+1)}\sqrt{J(J+1) - M(M+1)} \\ \langle J+1KM|h_S|JKM\rangle &= \cos\beta\sqrt{\frac{[(J+1)^2 - M^2][(J+1)^2 - K^2]}{(2J+3)(2J+1)(J+1)^2}} \\ \langle J+1KM+1|h_S|JKM\rangle &= -\frac{\sin\beta\sqrt{[(J+1)^2 - K^2](J+M+1)(J+M+2)}}{2(J+1)\sqrt{(2J+3)(2J+1)}} \\ \langle J+1KM-1|h_S|JKM\rangle &= -\langle J+1K-M+1|h_S|JK-M\rangle \end{aligned}$$

The laser Hamiltonian H_L (3) takes now the form

$$H_L = -\frac{I}{2\epsilon_0 c}h_L = -\frac{I}{2\epsilon_0 c}\left(\frac{\alpha^{zx} + \alpha^{yx}}{3} D^2_{00}(\Omega) - \frac{\alpha^{yx}}{\sqrt{6}}[D^2_{02}(\Omega) + D^2_{0-2}(\Omega)] + \frac{\alpha^{zx} + \alpha^{yx}}{3} \right). \tag{A8}$$

In this expression we have omitted the terms which only introduce a shift in the energy. Performing the integrals corresponding to each term, we get

$$\begin{aligned} \langle JKM|h_L|JKM\rangle &= \left(\frac{\alpha^{zx} + \alpha^{zy}}{3}\right)\frac{[3M^2 - J(J+1)][3K^2 - J(J+1)]}{2J(J+1)(2J-1)(2J+3)} + \frac{\alpha^{zx} + \alpha^{yx}}{3} \\ \langle J+1KM|h_L|JKM\rangle &= (\alpha^{zx} + \alpha^{zy})\frac{MK\sqrt{[(J+1)^2 - M^2][(J+1)^2 - K^2]}}{J(J+1)(J+2)\sqrt{(2J+3)(2J+1)}} \\ \langle J+2KM|h_L|JKM\rangle &= \left(\frac{\alpha^{zx} + \alpha^{zy}}{2}\right)\sqrt{[(J+2)^2 - K^2][(J+1)^2 - K^2]} \\ &\times\frac{\sqrt{[(J+2)^2 - M^2][(J+1)^2 - M^2]}}{(J+1)(J+2)(2J+3)\sqrt{(2J+1)(2J+5)}} \end{aligned}$$

$$\begin{aligned}
\langle JKM|h_L|JK+2M\rangle &= -\alpha^{yx}[3M^2 - J(J+1)] \\
&\quad \times \frac{\sqrt{[J^2-(K+1)^2](J-K)(J+K+2)}}{2J(J+1)(2J+3)(2J-1)} \\
\langle J+1KM|h_L|JK+2M\rangle &= -\alpha^{yx} M \sqrt{[(J+1)^2 - M^2]} \\
&\quad \times \frac{\sqrt{[(J-K)^2-1](J-K)(J+K+2)}}{2J(J+1)(J+2)\sqrt{(2J+1)(2J+3)}} \\
\langle J+2KM|h_L|JK+2M\rangle &= -\alpha^{yx} \sqrt{[(J+2)^2 - M^2][(J+1)^2 - M^2]} \\
&\quad \times \frac{\sqrt{[(J-K)^2-1](J-K)(J-K+2)}}{4(J+1)(J+2)(2J+3)\sqrt{(2J+1)(2J+5)}} \\
\langle J'K'M'|h_L|JKM\rangle &= \langle J'-K'-M'|h_L|J-K-M\rangle .
\end{aligned}$$

[1] H. J. Loesch and A. Remscheid, J. Chem. Phys. **93**, 4779 (1990).
[2] P. R. Brooks, Science **193**, 11 (1976).
[3] D. H. Parker and R. B. Bernstein, Annu. Rev. Phys. Chem. **40**, 561 (1989).
[4] T. D. Hain, R. M. Moision, and T. J. Curtiss, J. Chem. Phys. **111**, 6797 (1999).
[5] K. F. Lee, D. M. Villeneuve, P. B. Corkum, A. Stolow, and J. G. Underwood, Phys. Rev. Lett. **97**, 173001 (2006).
[6] M. D. Poulsen, T. Ejdrup, H. Stapelfeldt, E. Hamilton, and T. Seideman, Phys. Rev. A **73**, 033405 (2006).
[7] L. Holmegaard, J. H. Nielsen, I. Nevo, H. Stapelfeldt, F. Filsinger, J. Küpper, and G. Meijer, Phys. Rev. Lett. **102**, 023001 (2009).
[8] F. Filsinger, J. Küpper, G. Meijer, L. Holmegaard, J. H. Nielsen, I. Nevo, J. L. Hansen, and H. Stapelfeldt, J. Chem. Phys. **131**, 064309 (2009).
[9] I. Nevo, L. Holmegaard, J. Nielsen, J. L. Hansen, H. Stapelfeldt, F. Filsinger, G. Meijer, and J. Küpper, Phys. Chem. Chem. Phys. **11**, 9912 (2009).
[10] D. T. Moore, L. Oudejans, and R. E. Miller, J. Chem. Phys. **110**, 197 (1999).
[11] R. Kanya and Y. Ohshima, J. Chem. Phys. **121**, 9489 (2004).
[12] L. Holmegaard, J. L. Hansen, L. Kalhoj, S. L. Kragh, H. Stapelfeldt, F. Filsinger, J. Küpper, G. Meijer, D. Dimitrovski, M. Abu-samha, C. P. J. Martiny, and L. Madsen, Nat. Phys. **6**, 428 (2010).
[13] J. L. Hansen, L. Holmegaard, L. Kalhøj, S. L. Kragh, H. Stapelfeldt, F. Filsinger, G. Meijer, J. Küpper, D. Dimitrovski, M. Abu-samha, C. P. J. Martiny, and L. B. Madsen, Phys. Rev. A **83**, 023406 (2011).
[14] V. Aquilanti, M. Bartolomei, F. Pirani, D. Cappelletti, and F. Vecchiocattivi, Phys. Chem. Chem. Phys **7**, 291 (2005).
[15] P. R. Brooks and E. M. Jones, J. Chem. Phys. **45**, 3449 (1966).
[16] F. J. Aoiz, B. Friedrich, V. J. Herrero, V. S. Rábanos, and J. E. Verdasco, Chem. Phys. Lett. **289**, 132 (1998).
[17] R. Zare, Science **20**, 1875 (1998).
[18] M. Wu, R. J. Bemish, and R. E. Miller, J. Chem. Phys. **101**, 9447 (1994).
[19] R. Baumfalk, N. H. Nahler, and U. Buck, J. Chem. Phys. **114**, 4755 (2001).
[20] A. J. van den Brom, T. P. Rakitzis, and M. H. M. Janssen, J. Chem. Phys. **121**, 11645 (2004).
[21] M. L. Lipciuc, A. J. van den Brom, L. Dinu, and M. H. M. Janssen, Rev. Sci. Instrum. **76**, 123103 (2005).
[22] P. Reckenthaeler, M. Centurion, W. Fuß, S. A. Trushin, F. Krausz, and E. E. Fill, Phys. Rev. Lett. **102**, 213001 (2009).
[23] J. Levesque, Y. Mairesse, N. Dudovich, H. Pépin, J.-C. Kieffer, P. B. Corkum, and D. M. Villeneuve, Phys. Rev. Lett. **99**, 243001 (2007).
[24] R. Velotta, N. Hay, M. B. Mason, M. Castillejo, and J. P. Marangos, Phys. Rev. Lett. **87**, 183901 (2001).
[25] M. D. Poulsen, E. Péronne, H. Stapelfeldt, C. Z. Bisgaard, S. S. Viftrup, E. Hamilton, and T. Seideman, J. Chem. Phys. **121**, 783 (2004).
[26] J. J. Larsen, K. Hald, N. Bjerre, H. Stapelfeldt, and T. Seideman, Phys. Rev. Lett. **85**, 2470 (2000).
[27] M. Artamonov and T. Seideman, J. Chem. Phys. **128**, 154313 (2008).
[28] M. Artamonov and T. Seideman, Phys. Rev. A **82**, 023413 (2010).
[29] S. S. Viftrup, V. Kumarappan, S. Trippel, H. S. E. Hamilton, and T. Seideman, Phys. Rev. Lett. **99**, 143602 (2007).
[30] S. S. Viftrup, V. Kumarappan, L. Holmegaard, C. Z. Bisgaard, H. Stapelfeldt, M. Artamonov, E. Hamilton, and T. Seideman, Phys. Rev. A **79**, 023404 (2009).
[31] A. Schwettman, J. Franklin, K. R. Overstreet, and J. P. Shaffer, J. Chem. Phys. **123**, 194305 (2005).
[32] J. Bulthuis, J. Miller, and H. J. Loesch, J. Phys. Chem. A **101**, 7684 (1997).
[33] W. Kong and J. Bulthuis, J. Phys. Chem. A **104**, 1055 (2000).
[34] R. Kanya and Y. Ohshima, Phys. Rev. A **70**, 013403 (2004).

[35] M. Härtelt and B. Friedrich, J. Chem. Phys. **128**, 224313 (2008).
[36] I. N. Kozin and R. N. Roberts, J. Chem. Phys. **118**, 10523 (2003).
[37] W. Kim and P. M. Felker, J. Chem. Phys. **108**, 6763 (1998).
[38] B. Friedrich and D. Herschbach, J. Phys. Chem. A **103**, 10280 (1999).
[39] B. Friedrich and D. R. Herschbach, J. Chem. Phys. **111**, 6157 (1999).
[40] L. Cai, J. Marango, and B. Friedrich, Phys. Rev. Lett. **86**, 775 (2001).
[41] C. A. Arango and G. S. Ezra, Int. J. Bif. and Chaos **18**, 1127 (2008).
[42] J. J. Omiste, M. Gärttner, P. Schmelcher, R. González-Férez, L. Holmegaard, J. H. Nielsen, H. Stapelfeldt, and J. Küpper, Phys. Chem. Chem. Phys., accepted for publication(2011).
[43] R. N. Zare, *Angular momentum: understanding spatial aspects in chemistry and physics* (New York: John Wiley and Sons, 1988).
[44] C. M. Dion, A. Keller, O. Atabek, and A. D. Bandrauk, Phys. Rev. A **59**, 1382 (1999).
[45] N. E. Henriksen, Chem. Phys. Lett. **312**, 196 (1999).
[46] T. Seideman and E. Hamilton, *Nonadiabatic Alignment by Intense Pulses. Concepts, Theory, and Directions*, Advances In Atomic, Molecular, and Optical Physics, Vol. 52 (Academic Press, 2005) p. 289.
[47] G. W. King, R. M. Hainer, and P. C. Cross, J. Chem. Phys. **11**, 27 (1943).
[48] B. Bak, D. Christhensen, L. Hansen-Nygaard, and E. Tannenbaum, J. Chem. Phys. **26**, 134 (1957).
[49] K. J. Miller, J. Am. Chem. Soc. **112**, 8543 (1990).
[50] D. G. de Kowalewski, P. Kökeritz, and H. Sélen, J. Chem. Phys. **31**, 1438 (1959).
[51] K. K. Innes, I. G. Ross, and W. R. Moomaw, J. Mol. Spect. **132**, 492 (1988).
[52] A. Hinchliffe and H. J. Soscún M., J. M. Struct.-Theochem **304**, 109 (1994).
[53] H. Stapelfeldt and T. Seideman, Rev. Mod. Phys. **75**, 543 (2003).
[54] A. Rouzée, S. Guérin, O. Faucher, and B. Lavorel, Phys. Rev. A **77**, 043412 (2008).
[55] H. W. Kroto, *Molecular Rotation Spectra* (Dover Publications, Inc., New York, 1992).